Tribology Letters (2021) 69:45
https://doi.org/10.1007/s11249-021-01412-2

ORIGINAL PAPER

Investigation of the Tribological Performances of Graphene and WS_2 Nanosheets as Additives for Perfluoroalkylpolyethers Under Simulated Space Environment

Jia Ren[1,2] · Kuiliang Gong[1,3] · Gaiqing Zhao[1,3] · Wenjing Lou[1,3] · Xinhu Wu[1,4] · Xiaobo Wang[1,3]

Received: 1 December 2020 / Accepted: 7 February 2021 / Published online: 22 March 2021

Abstract

The tribological performances of perfluoroalkylpolyethers (PFPE) with graphene (Gr), WS_2, and the mixture of Gr and WS_2 (Gr + WS_2) before and after ultraviolet (UV), atomic oxygen (AO), and proton (Pr) irradiations were investigated. The composition and structure of PFPE, Gr, WS_2, and Gr + WS_2 were also analyzed to understand the effects of irradiation on the tribological behaviors of PFPE with additives. The results indicated that serious deterioration and degradation of PFPE took place and Gr was transformed to amorphous carbon after Pr irradiation, and surface oxidation of WS_2 occurred under the irradiations of AO and Pr. Moreover, compared to PFPE and PFPE additized with Gr and WS_2, PFPE with the addition of Gr + WS_2 exhibited excellent friction and wear reduction before and after UV and AO irradiations.

Graphical Abstract

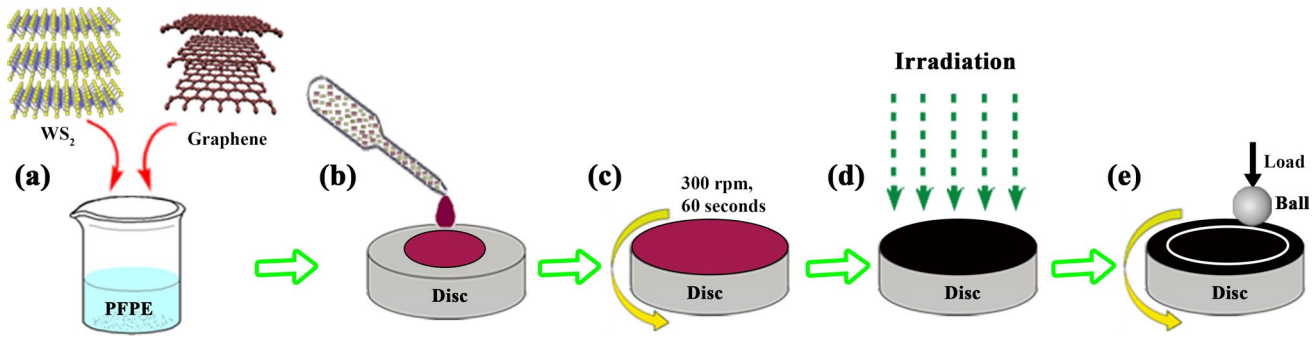

Keywords Lubricant additive · Graphene · WS_2 · Irradiation · Perfluoroalkylpolyethers

✉ Xinhu Wu
xinhu.wu@bristol.ac.uk

✉ Xiaobo Wang
wangxb@licp.cas.cn

[1] State Key Laboratory of Solid Lubrication, Lanzhou Institute of Chemical Physics, Chinese Academy of Sciences, Lanzhou 730000, People's Republic of China

[2] University of Chinese Academy of Sciences, Beijing 100049, People's Republic of China

[3] Qingdao Center of Resource Chemistry and New Materials, Qingdao 266000, China

[4] School of Chemistry, University of Bristol, Cantock's Close, Bristol BS8 1TS, UK

1 Introduction

With its significant influence on an overwhelming number of aerospace technical processes, the lubrication of moving mechanical components in the space environment has been a subject of intense scientific investigation [1]. While alternative space lubricants have been commercially available, selecting a high-performance lubricant to meet the growing demand for long-term and reliable operation of aerospace mechanisms still has been a challenging endeavor. Additionally, space lubrication presents problems which are not ordinarily encountered in the earth's atmosphere. The

unique effects to be considered include those of high vacuum (HV), radiation, temperature extremes, and weightlessness [2]. Among which, the radiation represents a fundamental obstacle to the application of conventional lubricants.

Perfluoroalkylpolyethers (PFPE), benefits from its chemical inertness, thermal stability, and low vapor pressure, has established itself as one of the best lubricants for space applications [3, 4]. However, there is still room for improvement in terms of the tribological properties of PFPE, especially under space environment [5]. Although a limited number of PFPE-soluble additives have been investigated [6, 7], these organic additives have not yet been used in space applications [8], which might attribute to their degradation under severe operating conditions. In recent years, inorganic nanoparticles (NPs) have shown great potential to replace the conventional organic additives because of their environmentally friendly, high thermal stability, and excellent friction-reducing and anti-wear (AW) characteristics [9]. Particularly, intensive research is carried out at using two-dimensional (2D) NPs as lubricating oil additives, such as graphene (Gr) and transition-metal dichalcogenides (TMDCs) [10–13]. In addition, the mixture of Gr and molybdenum disulfide (MoS_2) outperforms the individual Gr and MoS_2 NPs in comparison of friction and wear reduction due to their synergistic effect [14]. The favorable properties of graphene and TMDCs not only meet the requirement of sustainable development, but also enable them to be the most desirable lubricant additives for aerospace lubrication [15–18].

Previous research has study the tribological behaviors of ionic liquids (ILs) and multialkylated cyclopentanes (MACs) with various solid nanoparticles under simulated space environment [16–19], little is known with respect to improving the tribological properties of PFPE additized with nanoparticles at different irradiation conditions and investigating the effect of irradiation on the structure and physicochemical properties of nanoparticles. In this paper, the friction-reducing and AW properties of PFPE added with Gr, tungsten disulfide (WS_2), and the mixture of Gr and WS_2 were evaluated under ultraviolet (UV), atomic oxygen (AO), and proton (Pr) irradiations, respectively. The composition, structure, and morphology of these NPs added in PFPE before and after various irradiations were also investigated in detail.

2 Experimental Section

2.1 Materials

Fomblin YL VAC perfluoroalkylpolyethers (PFPE) was obtained from Solvay Solexis (Italy), and high-quality multilayer graphene (Gr) and tungsten disulfide (WS_2) ultrafine particles were purchased from Nanjing XFNANO Materials Tech Co., Ltd (China). AK-225, which is a mixture of 1,1-dichloro-2,2,3,3,3-pentafluoropropane and 1,3-dichloro-1,1,2,2,3-pentafluoropropane was obtained from Hunan Nonferrous Chenzhou Fluoride Chemical CO., LTD (China). Based on previous studies [10, 15], 1.0 wt% Gr, 1.0 wt% WS_2, and 0.5 wt% Gr + 0.5 wt%WS_2 were added to PFPE, respectively, and each additive was mixed thoroughly using magnetic stirrer for 30 min then subjected to ultrasonic treatment until a homogeneous dispersion was achieved (Scheme 1a).

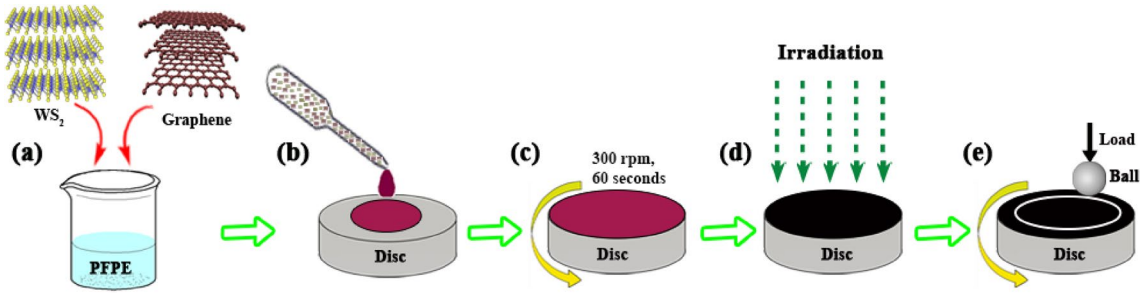

Scheme 1 The schematic of **a** preparation of PFPE with Gr + WS_2, **b**, **c** lubricant covering on the disc, **d** the irradiation process, and **e** the test configuration of ball-on-disc

Table 1 Experimental parameters of space irradiations

Irradiation mode	UV irradiation	AO irradiation	Pr irradiation
Irradiation parameters	100–400 nm, 800 W/cm^2	2.8×10^{15} atom/cm^2 s, 5 eV	2.5×10^{14} proton/cm^2 s, 25 kV
Irradiation time	30 min	30 min	10 min

2.2 Irradiation Procedure

UV, AO, and Pr irradiation experiments were carried out in ground-based simulation apparatus as reported elsewhere [16, 19]. As shown in Scheme 1, each of the lubricants was uniformly distributed on a steel substrate by rotating the disc, then the liquid layer was irradiated under vacuum conditions (better than 5.0×10^{-3} Pa). The experimental parameters and irradiation time are listed in Table 1. The simulated UV irradiation was produced by using a deuterium lamp and a xenon lamp as the light source, which can generate vacuum ultraviolet and near ultraviolet irradiation with energy levels of 800 W/m^2, and the radiation intensity was determined to be about 3 times larger than the solar constant. The AO simulated experiment was based on the microwave electron cyclotron resonance plasma technology. Oxygen was excited by a microwave power source to produce oxygen plasma, then the oxygen positive ions were extracted from the plasma and collided with the negative charges on the plate, forming a neutral AO beam with an impingement kinetic energy of 5 eV. The AO flux was 2.8×10^{15} atom/cm^2 s, and the exposure period was controlled as 30 min. The Pr irradiation provided the high-energy proton beam with an energy of 25 keV and the flux of 2.5×10^{14} cm^{-2} s^{-1} for 10 min.

To investigate the impact of irradiation on the composition and structure of PFPE base oil and nano-additives, the pure PFPE and the uniform dispersions of PFPE with different nanoparticles were irradiated, respectively. The base oil before and after irradiation was characterized by several techniques. The nano-additives were separated from the irradiated dispersions by removal of the PFPE oil with AK-225 solvent and were dried under vacuum over night before measurement.

2.3 Characterization of the Lubricants Before and After Irradiation

The chemical composition of PFPE oil and the three kind of nano-additives before and after irradiation were analyzed by a PHI-5702 multifunctional X-Ray photoelectron spectroscopy (XPS). The microstructures of Gr and WS_2 before and after irradiation were characterized using a FEI TECNAI F30 high-resolution transmission electron microscope (HR-TEM) at 300 kV. Raman spectra of Gr, WS_2, and the mixture of Gr and WS_2 (Gr + WS_2) before and after irradiation were recorded on a Thermo Scientific DXR Raman Microscope with a laser excitation wavelength of 532 nm.

The friction and wear tests for PFPE and PFPE with Gr, WS_2, and Gr + WS_2 before and after irradiation were carried out by a self-made rotational ball-on-disk apparatus under high vacuum (HV) at room temperature (20 ± 5 °C). The fixed upper specimens were the cleaned AISI 52,100 steel balls (hardness of ≈ 62 HRC, surface roughness Ra = 25 nm) with 6 mm in diameter, loaded against rotating discs (AISI 52,100 steel, ø 24.00 × 7.88 mm, hardness of ≈63 HRC, Ra = 43.6 nm). The tests parameters were set as: rotational radium of 6 mm, sliding speed of 500 r/min, normal loading force of 5 N, sliding time of 60 min, and vacuum degree of 10^{-4} Pa. The test was repeated three times for each lubricant. After the friction tests, worn surface morphologies of the steel discs were characterized by the MERLIN Compact field emission scanning electron microscopy (FE-SEM), and the wear tracks of the worn surface were investigated using a noncontact 3D surface profiler (AD Corporation, Massachusetts, USA). We then calculated the wear rates (K) by the formula [20]:

$$K = \frac{V}{SF}$$

where V is the wear volume, S is the total sliding distance, and F is the normal load.

Also, the wear scars on the steel ball were imaged by the DXR Raman Microscope, and the wear debris on the wear track were analyzed by Raman spectroscopy and PHI-5702 multifunctional XPS.

3 Results and Discussion

3.1 The Influence of Irradiation on the PFPE Base Oil

Photographs and weight losses of the PFPE base oil before and after irradiation are shown in Fig. 1. It is clear that the base oil showed little change in color and weight loss after UV and AO irradiations. In contrast, the PFPE oil exposed to Pr irradiation experienced a remarkable color change from colorless to dark brown and lost a significant weight. It is

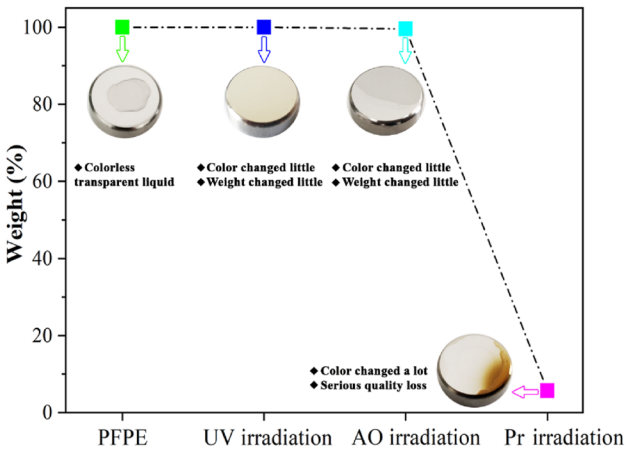

Fig. 1 UV, AO and Pr irradiation-induced changes in the weight and color of neat PFPE

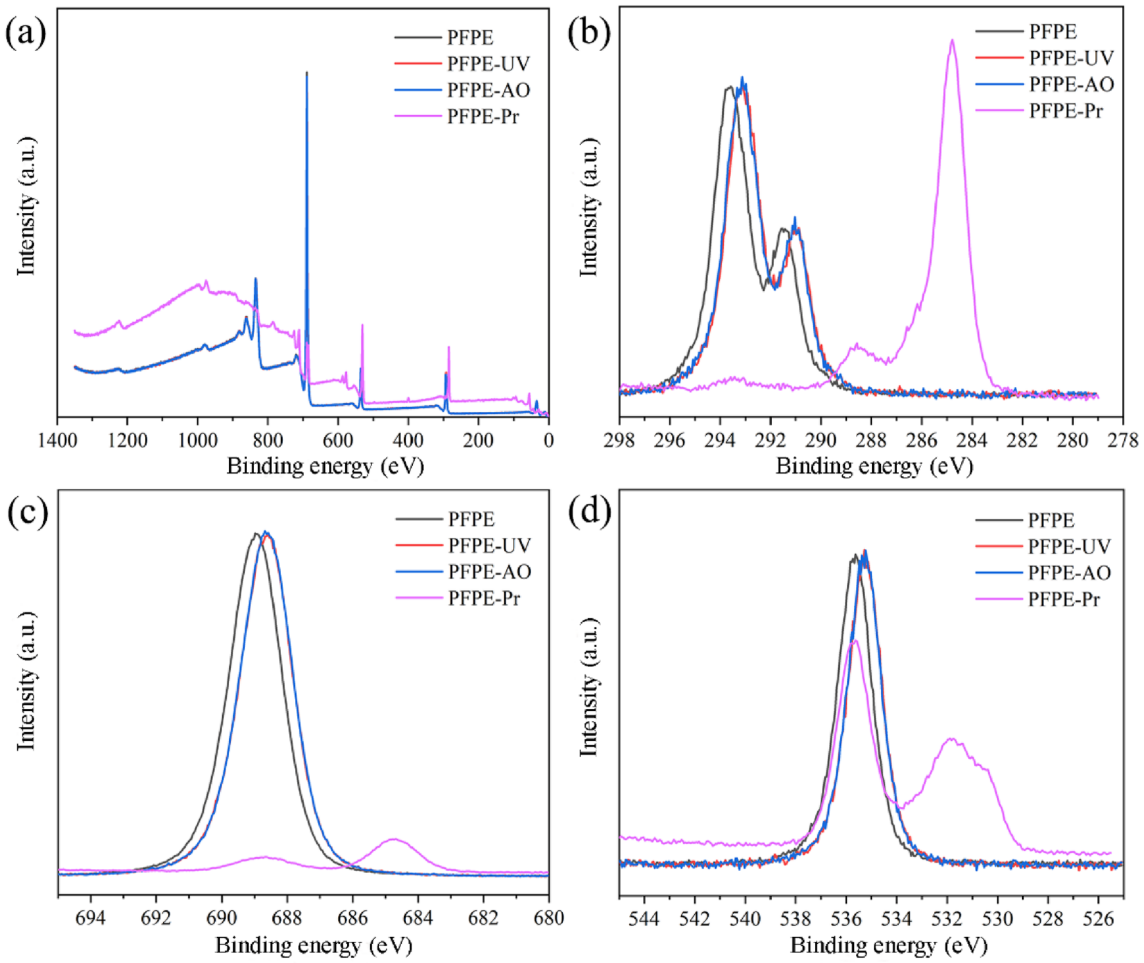

Fig. 2 XPS **a** survey spectra and high-resolution **b** C 1 s, **c** F 1 s, and **d** O 1 s spectra of PFPE before and after UV, AO, and Pr irradiations

indicated that decomposition reaction could take place and form new substances under Pr irradiation, resulting in the color becoming darker and weight loss [19].

The chemical composition of PFPE before and after irradiation was then analyzed by XPS, as shown in Fig. 2. Almost no difference is observed in XPS survey spectra (Fig. 2a) and high-resolution C 1 s, F 1 s and O1s spectra (Fig. 2b–d) of the PFPE oil before and after UV and AO irradiations, indicating that UV and AO irradiations have little influence on the base oil composition. But XPS spectra of the base oil have changed obviously after Pr irradiation, especially high-resolution spectra. From Fig. 2b, it can clearly be seen that the C1s peaks at about 293.6 and 291.5 eV attributing to $–CF_2–CF_2O–$ and $–CF_2O–$ units in the PFPE even disappeared entirely after Pr irradiation, and two new peaks emerged at 288.6 and 284.8 eV corresponding to $–CF_2–CH_2O–$ species and the amorphous carbon [21, 22]. This can be explained by the fact that H^+ could induce the cleavage of the C–F and C–C bonds and lead to the formation of C-H bond and amorphous carbon [21]. The result was further confirmed by the F1s XPS spectra (Fig. 2c), which shows that an intensive peak at about 690.0 eV ascribing to $–CF_2–CF_2O–$ and $–CF_2O–$ units of non-irradiated PFPE decreased dramatically and shifted to 688.7 eV that was assigned to the fluorine in a $–CF_2–CH_2O–$ structure after Pr irradiation and, at the same time, a new peak located at around 684.7 eV was also observed, which was attributed to the FeF_3 and

Table 2 Atomic composition of PFPE before and after irradiation

	C (Atomic %)	O (Atomic %)	F (Atomic %)	F/C	F/O
PFPE	26.35	9.49	64.16	2.43	6.76
PFPE-UV	26.41	9.45	64.14	2.43	6.78
PFPE-AO	26.52	9.36	64.12	2.42	6.85
PFPE-Pr	47.23	35.33	17.44	0.37	0.49

CrF_3 [22], suggesting that fluorine radicals formed during Pr irradiation could react with the surface of steel disc. In the O1s spectrum of Pr-irradiated PFPE (Fig. 2d), the intensity of the peak at 535.6 eV also deceased, accompanied with a new peak centered at 531.2 eV with a broad region from 533.8 to 529.0 eV, which implies that radicals generated from Pr irradiation process could further react with oxygen to form various oxygen-containing chemical groups (such as –OH and –CO) as they were exposed to air [21–23]. The above analyses indicate that UV and AO irradiations had no obvious effect on the structure and composition of PFPE, whereas Pr irradiation could break the PFPE chemical bonds, and resulted in a great defluorination and carbonization of the oil. In addition, the relative atomic concentrations and the values of F/C and F/O ratios of PFPE before and after UV, AO, and Pr irradiations are listed in Table 2. For instance, the F/C and F/O ratios of Pr-irradiated PFPE greatly decreased, which shown that most of the bonds including F element in the PFPE were broken during Pr irradiation, then forming small molecular substances and being gasified to surrounding circumstances. These data provide valuable insights into understanding how irradiation affects the structure and composition of PFPE, and the result is well consistent with those obtained from Fig. 2.

3.2 The Influence of Irradiation on Nano-Additives

The morphology and structure of Gr and WS_2 before and after UV, AO, and Pr irradiations were characterized by HR-TEM. Figure 3a shows the TEM image of pristine Gr, and inset is the HR-TEM image of the edge of Gr sheets, where more than ten layers of Gr are identified. Figure 3a` displays selected area electron diffraction (SAED) pattern of non-irradiated Gr, and the six-fold spot patterns are consistent with good quality graphene. The HR-TEM and SAED results of Gr after UV and AO exposure are shown in Fig. 3b,b` and c,c`, respectively. It is concluded that the morphology and crystal structure of Gr were nearly unchanged in response

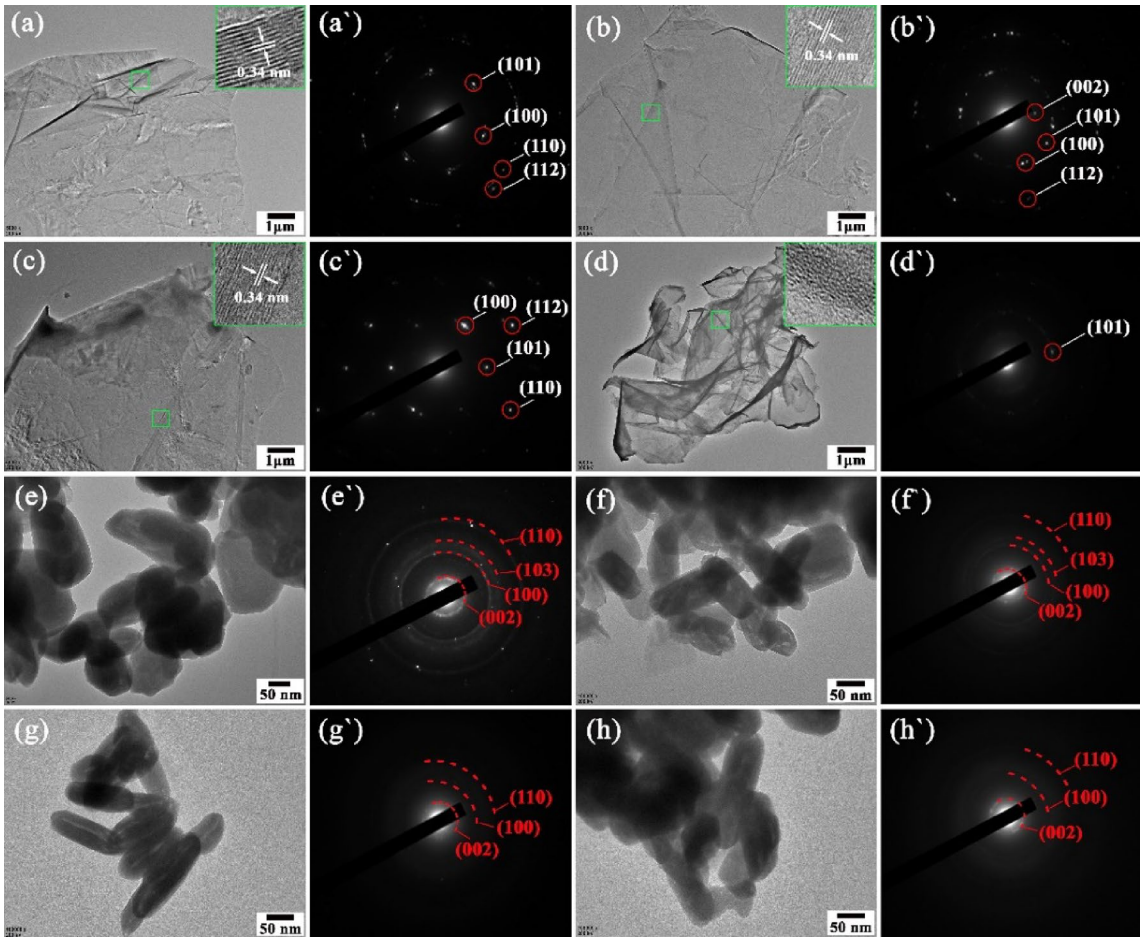

Fig. 3 TEM micrographs and SAED patterns of Gr and WS_2. (**a**, **a`**) pristine Gr, (**b**, **b`**) UV-irradiated Gr, (**c**, **c`**) AO-irradiated Gr, (**d**, **d`**) Pr-irradiated Gr, (**e**, **e`**) pristine $WS_2$, (**f**, **f`**) UV-irradiated WS_2, (**g**, **g`**) AO- irradiated $WS_2$, and (**h**, **h`**) Pr- irradiated WS_2. Insets of **a**, **b**, **c**, **d**: The HR-TEM micrographs of Gr before and after irradiations (zoomed from the green contour in **a**, **b**, **c**, **d**)

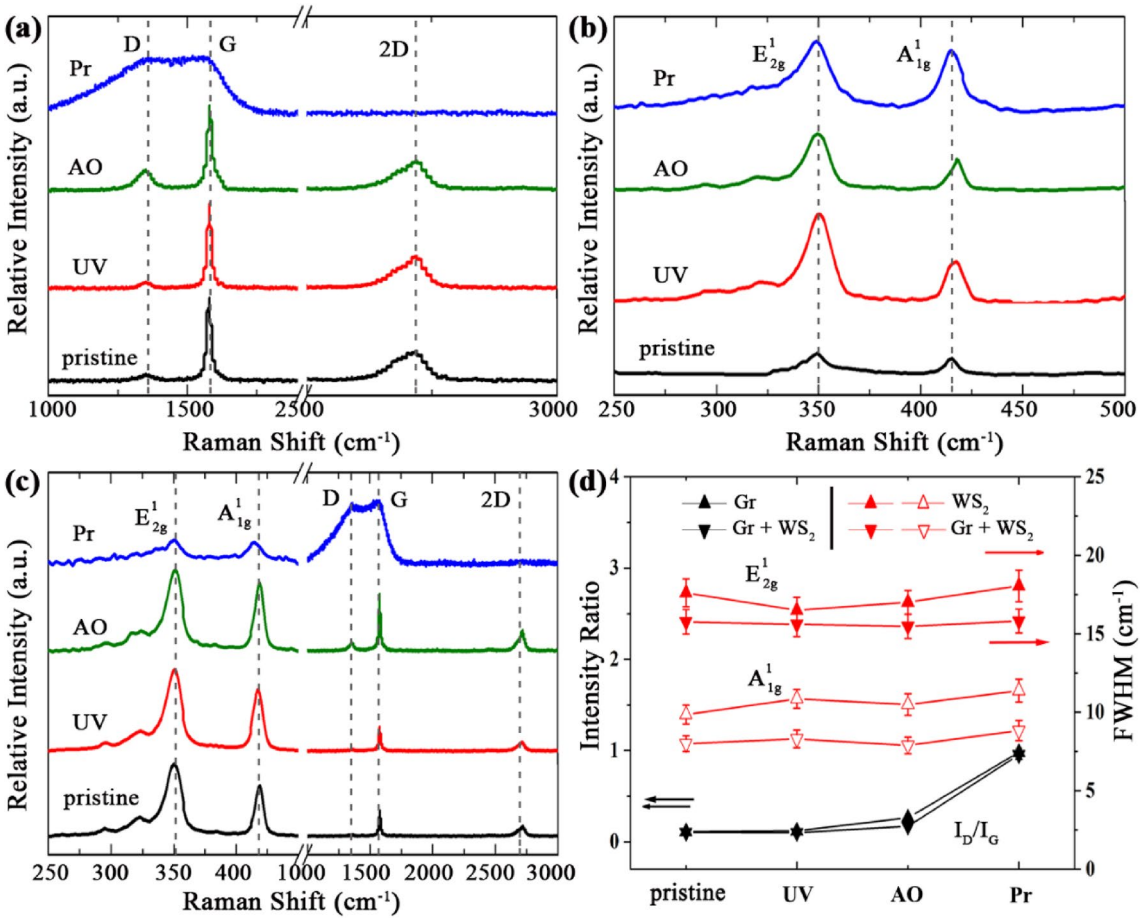

Fig. 4 Raman spectra of **a** Gr, **b** WS_2, and **c** Gr + WS_2 before and after UV, AO, and Pr irradiations. **d** The I_D/I_G ratios of Gr and Gr + WS_2, and the FWHM of WS_2 and Gr + WS_2 before and after irradiation

to UV and AO irradiations. However, the morphology of Gr has changed greatly after Pr irradiation as shown in Fig. 3d. The parallel Gr stripes are not visible in the HR-TEM image (inset in Fig. 3d), and the six-fold spot patterns are no longer observed in the SAED (Fig. 3d`), demonstrating that high quality Gr could be transformed into amorphous carbon with little or no remaining crystallinity under Pr beam exposure. Figure 2e,e`-2 h,h` respectively show the TEM images and SAED patterns of WS_2 before and after irradiations. It is seen that UV, AO, and Pr irradiations have no significant influence on the morphology and crystal structure of WS_2.

Raman spectroscopy has been employed extensively to characterize 2D materials such as Gr and transition metal dichalcogenides (TMDCs) [24]. Figure 4a represents the Raman spectra of Gr before and after UV, AO, and Pr irradiations. The spectra of pristine Gr and UV-irradiated Gr are similar to each other. However, the defect-activated D band (~1324 cm^{-1}) of AO-irradiated Gr can be observed with increased intensity relative to the G band (~1529 cm^{-1}) intensity (intensity ratios of I_D/I_G are shown in Fig. 4d), indicating that AO irradiation has certain effect on the structure of Gr. In stark contrast, the spectrum of Pr-irradiated Gr shows a shoulder peak of the D band with a nearly equal intensity to that of the G band, and the disappearance of the 2D band which is sensitive to the number of Gr layers. This result further confirms that Pr-irradiated Gr has been transformed into amorphous carbon [24]. In Fig. 4b, it was found that there was no obvious change in the Raman-active modes E^1_{2g} and A^1_{1g} of WS_2 before and after UV, AO, and Pr irradiations. But the full width at half-maximum (FWHM) of the corresponding two modes E^1_{2g} and A^1_{1g} in WS_2 shows that these two characteristic peaks become broad after AO and Pr irradiations (Fig. 4d), reflecting that AO and Pr beams induced disordering of WS_2. Benefitting from Gr covering the WS_2 surface [14], compositional disordering of WS_2 induced by Pr irradiation is not observed in the Raman spectra of Gr + WS_2 (Fig. 4c and d), but WS_2 could not prevent Gr from being irradiated into amorphous carbon.

The high-resolution XPS spectra of pristine WS_2 and the obtained WS_2 after UV, AO, and Pr irradiations are shown in Fig. 5. In each subplot, the XPS spectra of UV-irradiated WS_2 are similar to that of pristine WS_2. However, the

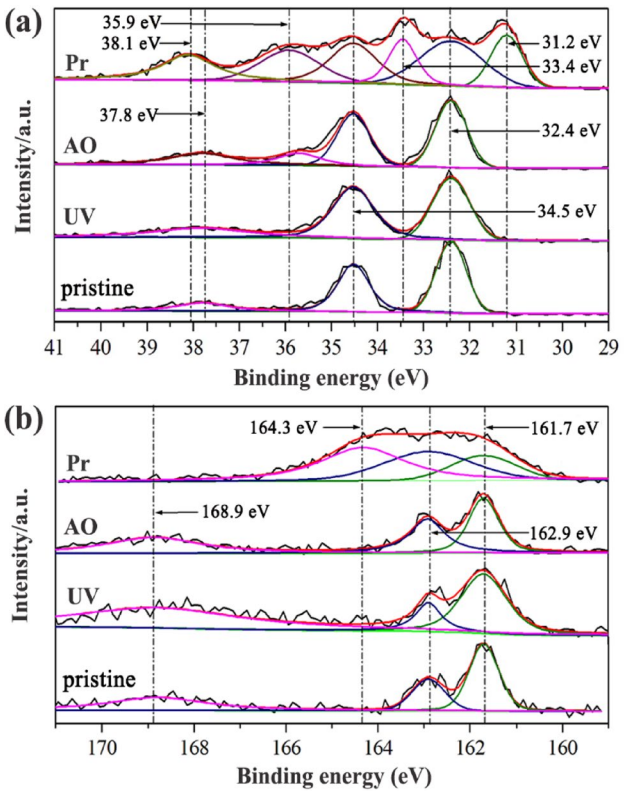

Fig. 5 XPS high-resolution **a** W 4f and **b** S 2p spectra of WS_2 before and after UV, AO, and Pr irradiations

shapes of W 4f and S 2p spectra for AO and Pr-irradiated WS_2 are changed dramatically, exhibiting that the compositions of WS_2 are affected by AO and Pr irradiations. For the AO-irradiated WS_2, the deconvolution of W 4f and S 2p spectra respectively show four peaks (Fig. 5a) and three peaks (Fig. 5b), which could be attributed to WS_2 (32.4 and 34.5 eV), WO_3 (35.9 and 37.8 eV), and WS_2 (161.7 and 162.9 eV), SO_4^{2-} (168.9 eV) [22, 25]. The W 4f and S 2p spectra of Pr-irradiated WS_2 respectively display six peaks (Fig. 5a) and three peaks (Fig. 5b), which were assigned to W (31.2 eV), WS_2 (32.4 and 34.5 eV), WO_2 (33.4 eV), WO_3 (35.9 and 38.1 eV), and WS_2 (161.7 and 162.9 eV), WS_3 (164.3 eV). These results indicate that surface oxidation of WS_2 can occurred when the material is irradiated with AO and Pr beams, causing compositional disordering of WS_2 layered structure, which is consistent with the result described in Fig. 4.

3.3 Tribological Properties of PFPE with Nano-Additives Before and After Irradiation

The tribological performances of PFPE and PFPE with 1%Gr, 1%WS_2, and 0.5%Gr + 0.5%WS_2 before and after UV, AO, and Pr irradiations were investigated under HV condition, and the friction testing results are shown in Fig. 6. Compared with the use of PFPE base oil, addition of Gr, WS_2 and Gr + WS_2 could eliminate the friction coefficient by ~15%, ~38%, and ~54%, respectively (Fig. 6a), implying the excellent friction reduction property of these three types of additives and the superior property of Gr + WS_2 than the others, the latter is mainly attributed to the synergy between Gr and WS_2 [14, 15]. After UV and AO irradiations (Fig. 6b and c), the base oils exhibit lower friction coefficients in comparison with the pristine PFPE, the possible reason is that UV and AO beams have no obvious effect on the structure and composition of PFPE and can increase the wettability and interfacial adhesion of PFPE on the surface of stainless steel [19], benefiting to reduce the friction coefficient. Because Gr, WS_2, and Gr + WS_2 have changed little after UV irradiation, there is a similar tendency and a slight decrease for the friction curves of UV-irradiated PFPE with Gr, WS_2, and Gr + WS_2 as compared to that of the pristine PFPE with these additives (Fig. 6b). Although the addition of Gr cannot effectively reduce the friction coefficient of PFPE after AO irradiation, and AO-irradiated PFPE with WS_2 shows an unstable frictional behavior, AO-irradiated PFPE with Gr + WS_2 displays a very low and stable friction curve (Fig. 6c), which might be due to the fact that Gr covers the surface of WS_2 and prevents the oxidation of WS_2 during AO irradiation, and has a synergistic effect with WS_2 in PFPE during rubbing. For Pr irradiation (Fig. 6d), serious deterioration and degradation of PFPE base oil and amorphization of graphene took place after Pr irradiation, resulting in the poor friction performances of PFPE, PFPE with Gr, and PFPE with Gr + WS_2. PFPE with WS_2 is significantly more effective than the others for friction reduction thanks to the excellent tribological properties of WS_2 under HV condition [26], but with randomly varying friction coefficient might be ascribed to the degradation of PFPE base oil.

After the friction tests, the corresponding wear rates of steel disc were calculated, and the results are shown in Fig. 7. It can be seen that the wear rates of PFPE and PFPE with different additives were increased after UV, AO, and Pr irradiations, particularly for Pr irradiation. Moreover, addition of Gr, WS_2, and Gr + WS_2 can effectively improve the AW performance of PFPE base oil both before and after irradiation, and the wear rates of the disc increase in the following order: Gr + WS_2 < Gr < WS_2 < PFPE. Despite their poor friction reduction performances, Gr and amorphous carbon transformed from Gr under Pr irradiation, suppressed abrasive, adhesive, and corrosive degradations effectively, and prevented wear [27, 28]. WS_2 exhibits excellent friction and wear resistance in vacuum, but the oxidation of WS_2 under AO and Pr irradiations, and during the sliding process, can

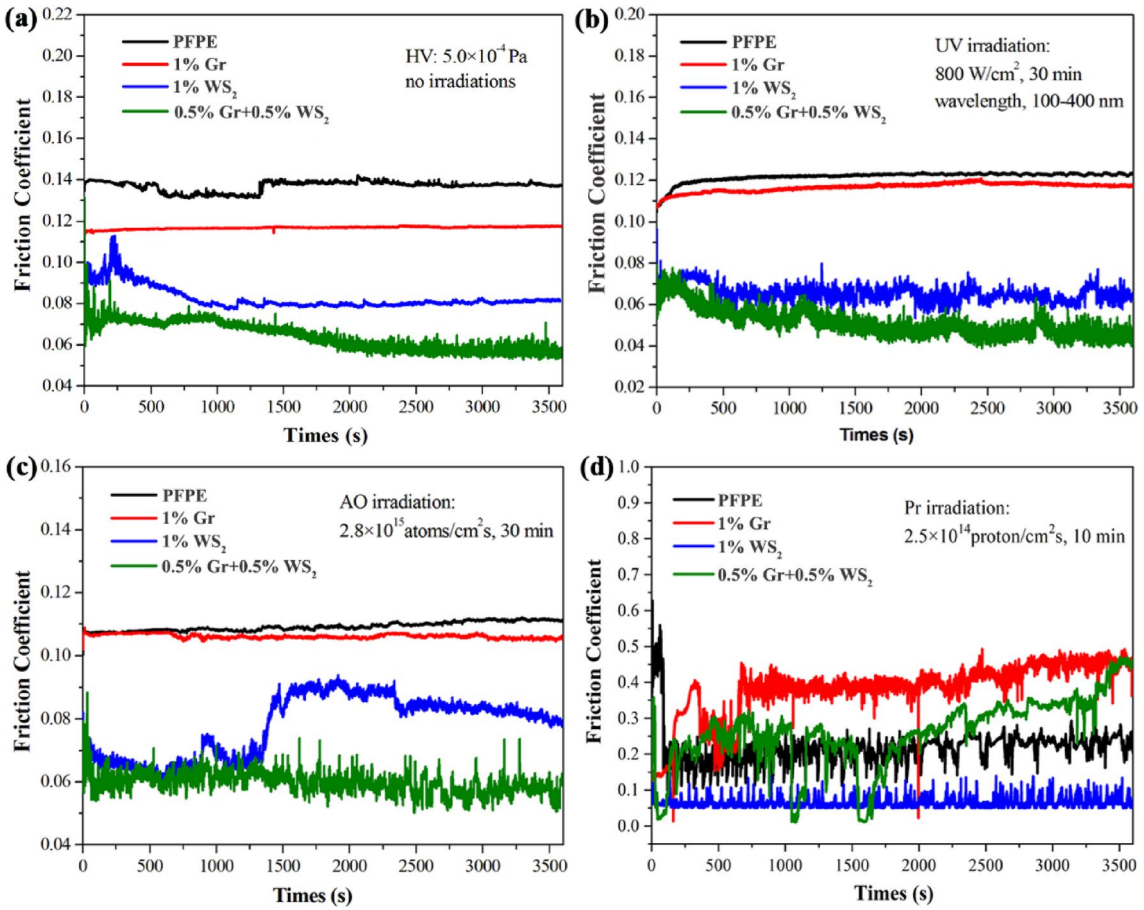

Fig. 6 Friction coefficient of PFPE and PFPE with 1% Gr, 1% WS_2, and 0.5% Gr + 0.5% WS_2 **a** before and after **b** UV, **c** AO, and **d** Pr irradiations

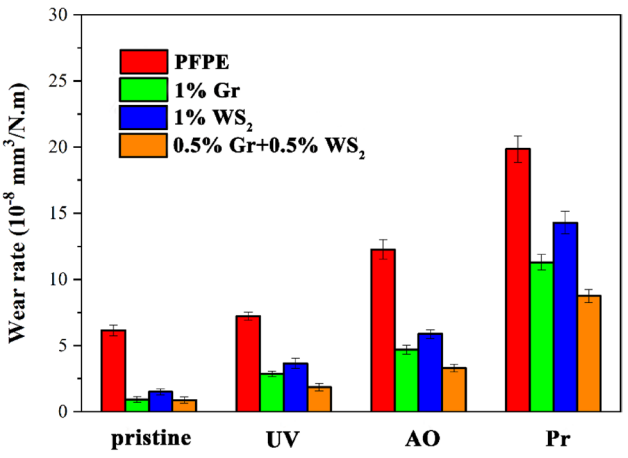

Fig. 7 The corresponding wear rates of steel disc lubricated by PFPE and PFPE with 1% Gr, 1% WS_2, and 0.5% Gr + 0.5% WS_2 before and after UV, AO, and Pr irradiations

cause the material to stick, resulting in rapid deterioration of its low-shear-strength properties. The oxides also lead to abrasive wear that aggravates wear and surface damage. Meanwhile, lowest wear rates of Gr + WS_2 compared with the other two additives are attributed to the formation of boundary lubrication film consisting graphene, amorphous carbon and WS_2 [29], which will be greatly beneficial for wear protection.

The wear situation of material pairs was further observed with SEM and optical microscopy. In Fig. 8, the trend showed by SEM micrograph of the wear track on the disc was consistent with the results of wear rates. The optical images of corresponding wear track on the steel ball are shown in Fig. 9. It is clear that the wear scar diameters of steel ball with Gr, WS_2, and Gr + WS_2 at the sliding interface were significantly decreased when compared to that of ball lubricated by pristine PFPE before and after UV, AO, and

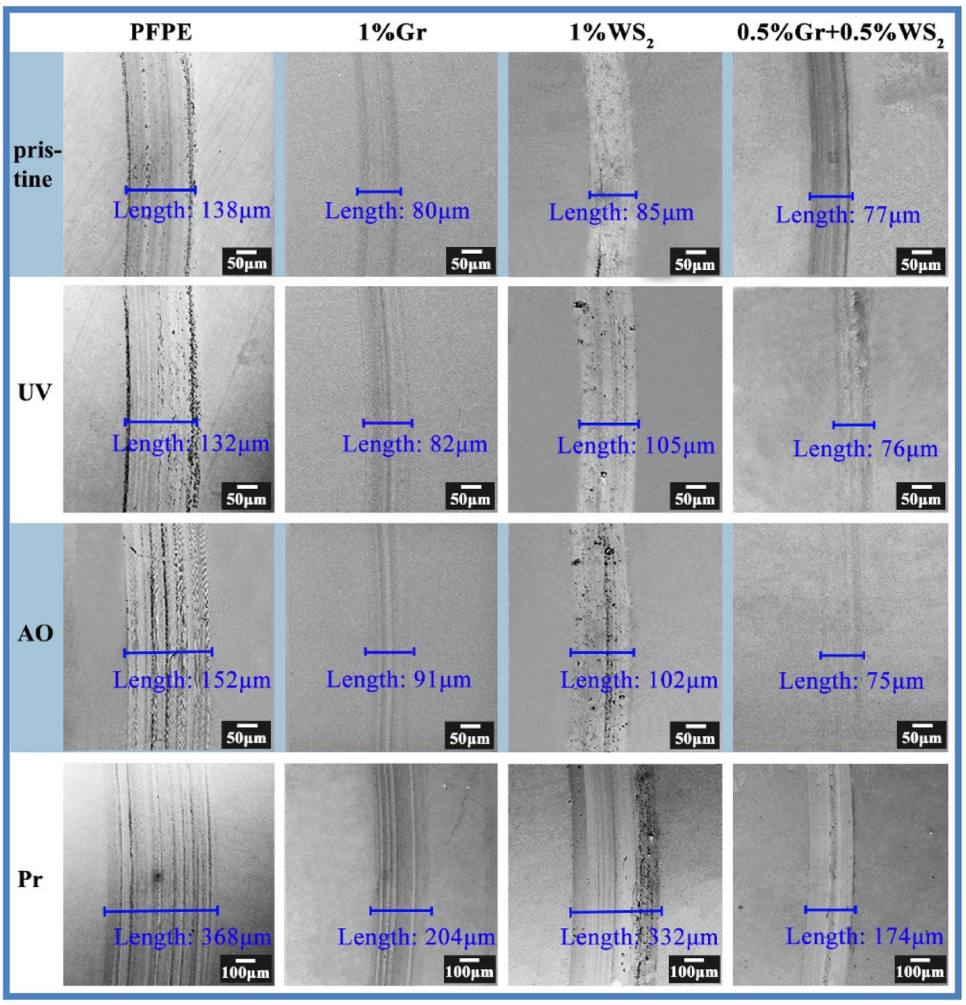

Fig. 8 SEM images of the corresponding wear surface of steel disc lubricated by PFPE and PFPE with 1% Gr, 1% WS_2, and 0.5% Gr + 0.5% WS_2 before and after UV, AO, and Pr irradiations

Pr irradiations, particularly the wear damage was minimal with Gr + WS_2 at the sliding interface (as shown in Fig. 9d, h, l, p, respectively). However, the steel ball was damaged the most seriously by Pr irradiation in comparison with that by the two other irradiations. In addition to showing similar wear situation to that of steel disc, the optical images of wear scar on steel ball indicated the presence of wear debris, which were analyzed by Raman spectroscopy and XPS to understand the lubrication mechanism involved.

3.4 The Lubrication Mechanism of PFPE with Nano-Additives Before and After Irradiation

Figure 10 shows the Raman analysis inside the corresponding wear track in Fig. 9. The analyses inside the wear scar on the ball with pristine PFPE and irradiated-PFPE at the sliding interface (Fig. 10a) confirm the presence of amorphous carbon in the wear debris, and Raman analyses of wear scar on the steel ball lubricated by PFPE with Gr (Fig. 10b), PFPE with WS_2 (Fig. 10c) and PFPE with Gr + WS_2 (Fig. 10d) before and after UV, AO irradiations confirm the presence of Gr and amorphous carbon, WS_2 and amorphous carbon, and Gr, WS_2 and amorphous carbon within the wear tracks, respectively, while the analyses of wear scar on the ball lubricated by these lubricants after Pr irradiation confirm the presence of amorphous carbon (Fig. 10b) and WS_2 and amorphous carbon (Fig. 10c and d), respectively.

The wear scars in Fig. 10 were also characterized by XPS. As shown in Fig. 11a, the binding energies of C 1 s of the worn surface lubricated by PFPE and PFPE with WS_2 before and after UV, AO and Pr irradiations are similar to each other, and the spectra display three main peaks centered at

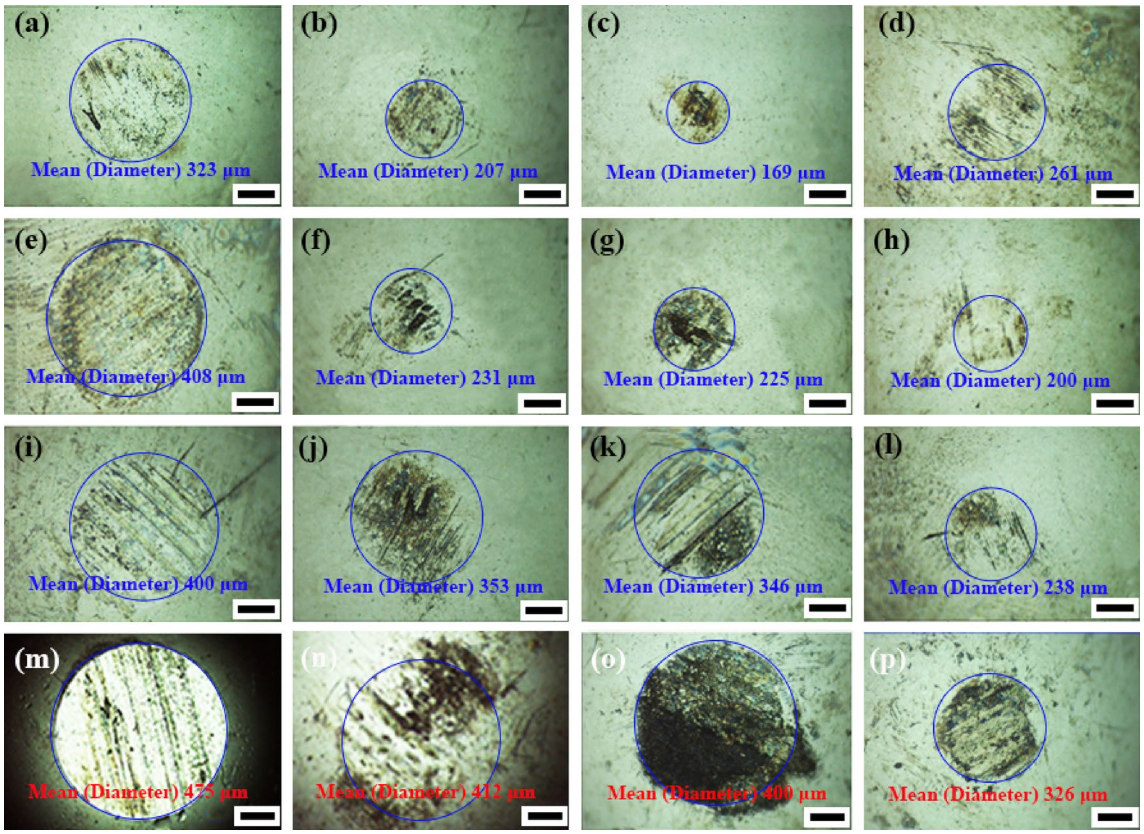

Fig. 9 Optical microscopy images of the corresponding wear scar on the steel ball lubricated by (**a**, **e**, **i**, **m**) PFPE and PFPE with (**b**, **f**, **j**, **n**) 1% Gr, (**c**, **g**, **k**, **o**) 1% WS_2, and (**d**, **h**, **l**, **p**) 0.5% Gr + 0.5% WS_2 (**a**–**d**) before and after (**e**–**h**) UV, (**i**–**l**) AO, and (**m**–**p**) Pr irradiations. The scale bar indicates 100 µm in all images

284.8 eV, 291.5 eV, and 293.6 eV, which were assigned to the -C–C- of amorphous carbon species, carbon from the repeating -CF_2-CF_2O- and -CF_2O- units in PFPE chains [21, 22]. However, the C 1 s spectra of worn surface lubricated by PFPE with Gr and PFPE with Gr + WS_2 before and after these irradiations show similar peaks located at 284.8 eV, and the disappearance of peaks at 291.5 eV and 293.6 eV might be due to the covering of PFPE surface with Gr or amorphous carbon. Figure 11b shows one peak of F 1 s at about 689.2 eV, corresponding to organic oxyfluoride or carbon fluoride species [30], the difference is that the intensities have decreased significantly when the friction pairs were lubricated by PFPE with Gr and Gr + WS_2 before and after various irradiations. The W 4f spectra of wear scar on the ball lubricated by PFPE with WS_2 and PFPE with Gr + WS_2 before and after UV, AO, and Pr irradiations show two peaks centered at about 35 eV and 37 eV (Fig. 11c, d), which were assigned to WS_2 and WO_3. Similarly, the intensities of the two peaks of wear scar on the ball lubricated by PFPE with Gr + WS_2 are dramatically lower in comparison with PFPE with WS_2.

The above Raman and XPS analyses reveal that the presence of Gr or graphitic carbon can prevent the deterioration of PFPE base oil and oxidation of WS_2 before and after irradiation, and during sliding process, forming a stable boundary lubrication film on the rubbed surface, the protection film composed of Gr, amorphous carbon, WS_2, and PFPE species, which contributes to the excellent AW behavior of PFPE with Gr + WS_2 under irradiation.

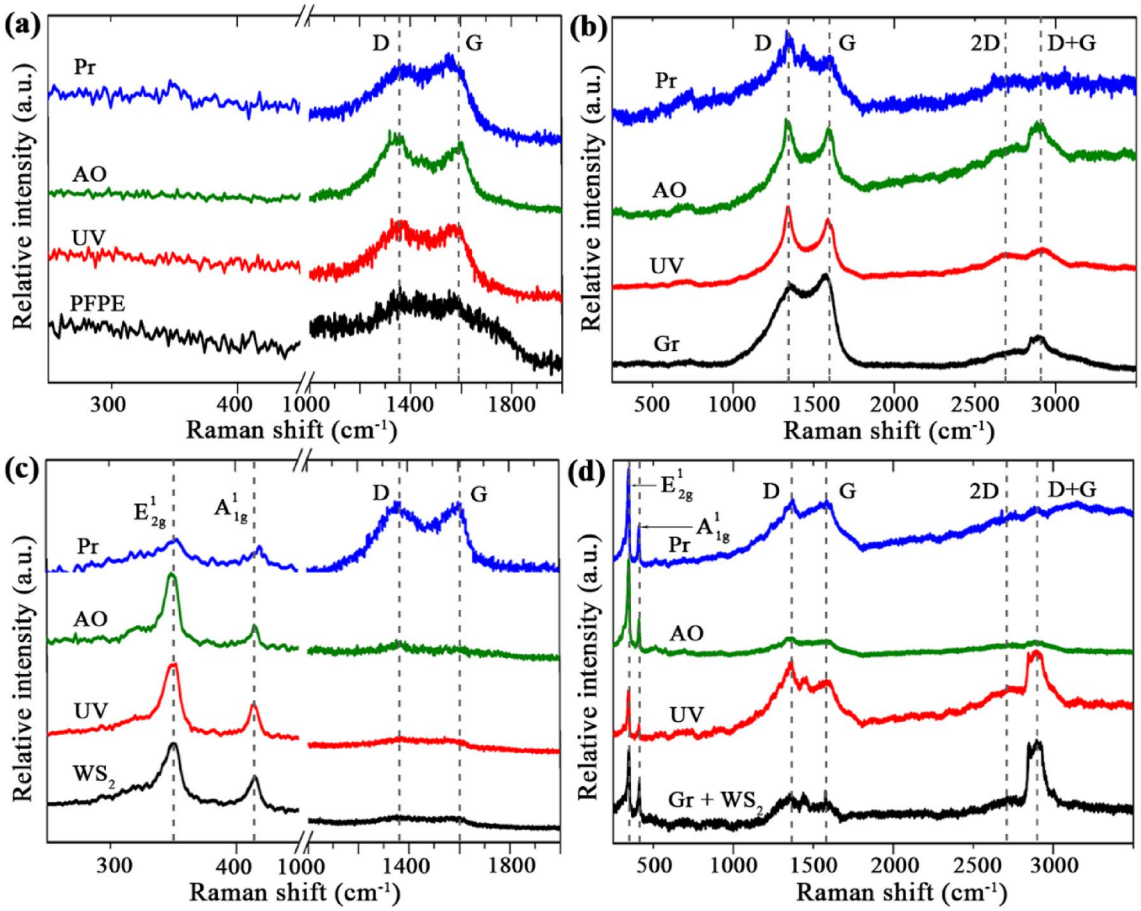

Fig. 10 Raman analysis of the corresponding wear scar on the steel ball lubricated by **a** PFPE, and PFPE with **b** Gr, **c** WS_2, and **d** Gr + WS_2 before and after UV, AO, and Pr irradiations

4 Conclusions

The impacts of UV, AO, and Pr irradiations on the composition and structure of PFPE base oil and the nano-additives of Gr, WS_2, and Gr + WS_2 were investigated, respectively. Moreover, the tribological performances of PFPE and PFPE with Gr, WS_2, and Gr + WS_2 before and after the irradiations were evaluated, and Raman and XPS techniques were used to explore the lubrication mechanism. The results of this study indicated that:

The composition and structure of PFPE base oil were almost unchanged after UV and AO irradiations, but serious deterioration and degradation of PFPE base oil took place after Pr irradiation.

Similarly, UV and AO irradiations have little effect on the composition and morphology of Gr. However, Pr irradiation can transform Gr into amorphous carbon. As WS_2 was exposed to the simulated space radiations except for UV irradiation, surface oxidation of WS_2 could occurred, inducing compositional disordering of WS_2 layered structure.

Benefitting from the synergistic effect between Gr and WS_2, PFPE with Gr + WS_2 exhibited the lowest friction coefficient than the base oil and the oil with Gr and WS_2 before and after UV and AO irradiations, and displayed the excellent wear rates compared with that of PFPE and PFPE with Gr and WS_2 before and after UV, AO, and Pr irradiations.

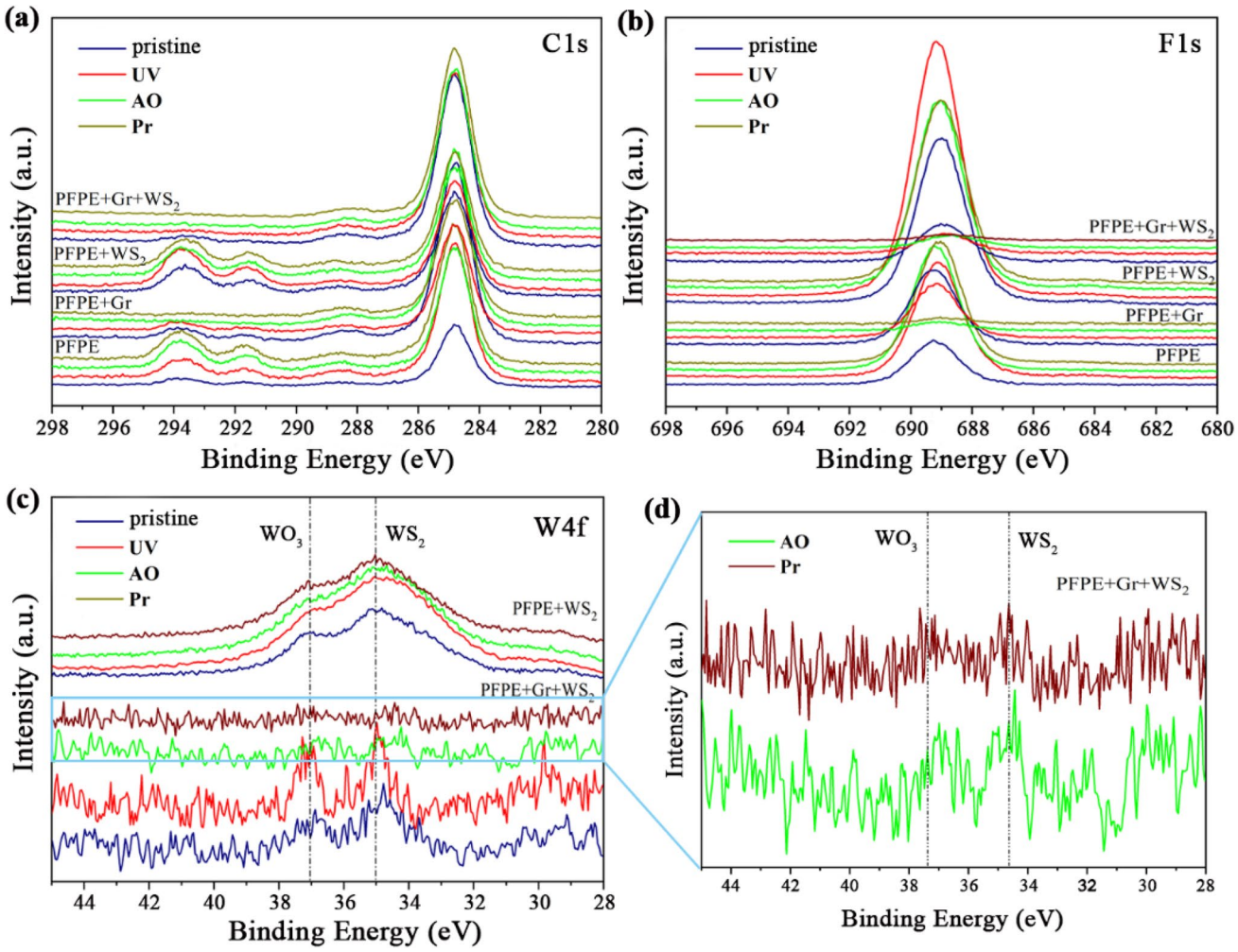

Fig. 11 XPS high-resolution **a** C 1 s, **b** F 1 s and **c**, **d** W 4f spectra of wear scar on the steel ball lubricated by PFPE, and PFPE with Gr, WS_2, and Gr + WS_2 before and after UV, AO, and Pr irradiations

Acknowledgements The authors are thankful for financial support of this work by National Key Research and Development Program of China (2018YFB2000601) and National Natural Science Foundation of China (NSFC 51875553)

Compliance with Ethical Standards

Conflict of interest The authors declare no competing financial interest.

References

1. Wolfberger, A., Zehl, M., Hausberger, A., Tockner, M., Schlögl, S., Hołyńska, M., Semprimoschnig, C.: Effect of accelerated aging on the chemical signature and performance of a multiply-alkylated cyclopentane (MAC) lubricant for space applications. Tribol. Lett. **69**, 3 (2021)
2. Zaretsky, E.V.: Liquid lubrication in space. Tribol. Int. **23**, 75–93 (1990)
3. Lv, M., Yang, L.J., Wang, Q.H., Wang, T.M., Liang, Y.M.: Tribological performance and lubrication mechanism of solid–liquid lubricating materials in high-vacuum and irradiation environments. Tribol. Lett. **59**, 20 (2015)
4. Srinivasan, P., Corti, C., Montagna, L., Savelli, P.: Soluble additives for perfluorinated lubricants. Lubr. Sci. **10**, 143–164 (1993)

5. Rudnick, L.R., Shubkin, R.L.: Synthetic lubricants and high-performance functional fuids, revised and expanded, Bell GA, Howell J, Del Pesco TW. Perfuoroalkylpolyethers. Crc Press, 218–223 (1999).
6. Zhu, J.M., Liang, Y.M., Liu, W.M.: Effect of novel phosphazene-type additives on the tribological properties of Z-DOL in a steel-on-steel contact. Tribol. Int. **37**, 333–337 (2004)
7. Masuko, M., Takeshita, N., Okabe, H.: Evaluation of anti-wear performance of PFPE soluble additives under sliding contact in high vacuum. Tribol. Trans. **38**, 679–685 (1995)
8. Jones, W.R., Jr., Jansen, M.J.: Tribology for space applications. P. I. Mech. Eng. J-J Eng. **222**, 997–1004 (2008)
9. Erdemir, A., Ramirez, G., Eryilmaz, O.L., Narayanan, B., Liao, Y.F., Kamath, G., Sankaranarayanan, S.K.R.S.: Carbon-based tribofilms from lubricating oils. Nature **536**, 67–71 (2016)
10. Zhao, J., He, Y.Y., Wang, Y.F., Wang, W., Yan, L., Luo, J.B.: An investigation on the tribological properties of multilayer graphene and MoS_2 nanosheets as additives used in hydraulic applications. Tribol. Int. **97**, 14–20 (2016)
11. Njiwa, P., Hadj-Aïssa, A., Afanasiev, P., Geantet, C., Bosselet, F., Vacher, B., Belin, M., Mogn, T., Dassenoy, F.: Tribological properties of new MoS2 nanoparticles prepared by seed-assisted solution technique. Tribol. Lett. **55**, 473–481 (2014)
12. Rabaso, P., Ville, F., Dassenoy, F., Diaby, M., Afanasiev, P., Cavoret, J., Vacher, B., Mogne, T.L.: Boundary lubrication: influence of the size and structure of inorganic fullerene-like MoS_2 nanoparticles on friction and wear reduction. Wear **320**, 161–178 (2014)
13. Chen, Z., Liu, X.W., Liu, Y.H., Gunsel, S., Luo, J.B.: Ultrathin MoS_2 nanosheets with superior extreme pressure property as boundary lubricants. Sci. Rep. **5**, 12869 (2015)
14. Xu, Y.F., Peng, Y.B., Dearn, K.D., Zheng, X.J., Yao, L.L., Hua, X.G.: Synergistic lubricating behaviors of graphene and MoS_2 dispersed in esterified bio-oil for steel/steel contact. Wear **342–343**, 297–309 (2015)
15. Wu, X.H., Zhao, G.Q., Zhao, Q., Gong, K.L., Wang, X.B., Liu, W.M., Liu, W.S.: Investigating the tribological performance of nanosized MoS_2 on graphene dispersion in perfluoropolyether under high vacuum. RSC Adv. **6**, 98606–98610 (2016)
16. Fan, X.Q., Wang, L.P., Li, W., Wan, S.H.: Improving tribological properties of multialkylated cyclopentanes under simulated space environment: two feasible approaches. ACS Appl. Mater. Interfaces. **7**, 14359–14368 (2015)
17. Fan, X.Q., Wang, L.P.: Graphene with outstanding anti-irradiation capacity as multialkylated cyclopentanes additive toward space application. Sci. Rep. **5**, 12734 (2015)
18. Zhang, S.W., Hu, L.T., Wang, H.Z., Feng, D.P.: The anti-seizure effect of Ag nanoparticles additive in multialkylated cyclopentanes oil under vacuum condition. Tribol. Int. **55**, 1–6 (2012)
19. Liu, X.F., Wang, L.P., Pu, J.B., Xue, Q.J.: Surface composition variation and high-vacuum performance of DLC/ILs solid–liquid lubricating coatings: Influence of space irradiation. Appl. Surf. Sci. **258**, 8289–8297 (2012)
20. Cai, M.R., Liang, Y.M., Zhou, F., Liu, W.M.: Tribological properties of novel imidazolium ionic liquids bearing benzotriazole group as the antiwear/anticorrosion additive in poly(ethylene glycol) and polyurea grease for steel/steel contacts. ACS Appl. Mater. Interfaces **3**, 4580–4592 (2011)
21. Lv, M., Zheng, F., Wang, Q.H., Wang, T.M., Liang, Y.M.: Surface structural changes, surface energy and antiwear properties of polytetrafluoroethylene induced by proton irradiation. Mater. Design. **85**, 162–168 (2015)
22. NIST X-ray Photoelectron Spectroscopy Database, version 4.1; National Institute of Standards and Technology, Gaithersburg, MD, 2012. http://srdata.nist.gov/xps/ Accessed March 2013
23. Griesser, H.J., Da, Y.X., Hughes, A.E., Gengenbach, T.R., Mau, A.W.H.: Shallow reorientation in the surface dynamics of plasma-treated fluorinated ethylene propylene polymer. Langmuir **7**, 2484–2491 (1991)
24. Maguire, P., Fox, D.S., Zhou, Y.B., Wang, Q.J., O'Brien, M., Jadwiszczak, J., Cullen, C.P., McManus, J., Bateman, S., McEvoy, N., Duesberg, G.S., Zhang, H.Z.: Defect sizing, separation, and substrate effects in ion-irradiated monolayer two-dimensional materials. Phys. Rev. B **98**, 134109 (2018)
25. Aldana, P.U., Dassenoy, F., Vacher, B., Mogne, T.L., Thiebaut, B.: WS_2 nanoparticles anti-wear and friction reducing properties on rough surfaces in the presence of ZDDP additive. Tribol. Int. **102**, 213–221 (2016)
26. Iwaki, M., Mogne, T.L, Fontaine, J., Martin, J.M., Watanabe, S., Noshiro, J.: Superlow friction of WS_2 coatings in ultrahigh vacuum at low temperature. WTC2005–63763, 931−932.
27. Berman, D., Erdemir, A., Sumant, A.V.: Approaches for achieving superlubricity in two-dimensional materials. ACS Nano **12**, 2122–2137 (2018)
28. Berman, D., Erdemir, A., Sumant, A.V.: Reduced wear and friction enabled by graphene layers on sliding steel surfaces in dry nitrogen. Carbon **59**, 167–175 (2013)
29. Kalyan, C.M., Wu, Y.A., Erdemir, A., Sumant, A.V.: Graphene-MoS_2 ensembles to reduce friction and wear in DLC-Steel contacts. Carbon **146**, 524–527 (2019)
30. Choa, S., Ludema, K.C., Potter, G.E., Dekoven, B.M., Morgan, T., Kar, K.K.: A model for the boundary film formation and tribological behavior of a phosphazene lubricant on steel. Tribol. Trans. **38**, 757–768 (1995)